

## Modeling transport and fate of riverine dissolved organic carbon in the Arctic Ocean

M. Manizza,<sup>1</sup> M. J. Follows,<sup>1</sup> S. Dutkiewicz,<sup>1</sup> J. W. McClelland,<sup>2</sup> D. Menemenlis,<sup>3</sup> C. N. Hill,<sup>1</sup> A. Townsend-Small,<sup>4</sup> and B. J. Peterson<sup>5</sup>

Received 8 October 2008; revised 5 June 2009; accepted 12 June 2009; published 7 October 2009.

[1] The spatial distribution and fate of riverine dissolved organic carbon (DOC) in the Arctic may be significant for the regional carbon cycle but are difficult to fully characterize using the sparse observations alone. Numerical models of the circulation and biogeochemical cycles of the region can help to interpret and extrapolate the data and may ultimately be applied in global change sensitivity studies. Here we develop and explore a regional, three-dimensional model of the Arctic Ocean in which, for the first time, we explicitly represent the sources of riverine DOC with seasonal discharge based on climatological field estimates. Through a suite of numerical experiments, we explore the distribution of DOC-like tracers with realistic riverine sources and a simple linear decay to represent remineralization through microbial degradation. The model reproduces the slope of the DOC-salinity relationship observed in the eastern and western Arctic basins when the DOC tracer lifetime is about 10 years, consistent with published inferences from field data. The new empirical parameterization of riverine DOC and the regional circulation and biogeochemical model provide new tools for application in both regional and global change studies.

**Citation:** Manizza, M., M. J. Follows, S. Dutkiewicz, J. W. McClelland, D. Menemenlis, C. N. Hill, A. Townsend-Small, and B. J. Peterson (2009), Modeling transport and fate of riverine dissolved organic carbon in the Arctic Ocean, *Global Biogeochem. Cycles*, 23, GB4006, doi:10.1029/2008GB003396.

### 1. Introduction

[2] The Arctic represents only 1% of the volume of the global ocean, but it receives ~10% of the entire global freshwater input [Opsahl *et al.*, 1999; Stein and MacDonald, 2003]. About half of the global inventory of organic carbon is stored in the drainage areas surrounding the Arctic Ocean. Dixon *et al.* [1994] and Dittmar and Kattner [2003] estimated that rivers convey ~18–26 Tg C a<sup>-1</sup> (1 Tg = 10<sup>12</sup> g) of DOC of terrestrial origin into the basin each year. As we learn more about the seasonality of organic matter export from Arctic rivers, these estimates are being revised upward. On the basis of a more complete database with finer temporal resolution, Raymond *et al.* [2007] showed that the five major Arctic rivers (Yenisey, Lena, Ob', Mackenzie, and Yukon) account for ~16 Tg C a<sup>-1</sup> and estimated that total DOC export from rivers to the Arctic Ocean is between 25 and 36 Tg C a<sup>-1</sup>, including all the

major Arctic rivers. This estimate of total DOC export was derived from a general relationship between DOC yield and water yield across the five major basins and is considered to be conservative because smaller basins confined to higher latitudes are likely to have higher DOC to water yield ratio [Raymond *et al.*, 2007].

[3] Large gradients of [DOC] are observed from coastal waters to those in the middle of the Arctic Basin reflecting this riverine source. Coastal surface DOC can reach 500 μM or more [Gordeev *et al.*, 1996; Lobbes *et al.*, 2000], dropping to less than 100 μM in the mid-Arctic Ocean surface waters. This trend is tightly coupled to gradients of salinity, which increases from the coastal zones to the middle of the basin. The DOC-salinity relationship (DSR) in the upper water column has been examined in several studies [Hansell *et al.*, 2004; Cooper *et al.*, 2005] and used as a tool for understanding the mixing processes between two distinct end-members: the coastal waters (fresher and rich in DOC) and the waters from the middle of the Arctic Basin (saltier and lower in DOC). On the basis of observed DSRs and interpretation of regional discharges and circulation, independent studies [Hansell *et al.*, 2004; Cooper *et al.*, 2005] have estimated that the lifetime for the microbial degradation [Azam and Hodson, 1977; Amon and Benner, 1996] and photolysis [Kieber *et al.*, 1990] of terrigenous DOC is between 4 and 10 years. Here we examine the interpretation of Hansell *et al.* [2004] in the context of a numerical ocean general circulation model

<sup>1</sup>Department of Earth, Atmospheric, and Planetary Sciences, Massachusetts Institute of Technology, Cambridge, Massachusetts, USA.

<sup>2</sup>Marine Science Institute, University of Texas at Austin, Port Aransas, Texas, USA.

<sup>3</sup>Jet Propulsion Laboratory, California Institute of Technology, Pasadena, California, USA.

<sup>4</sup>Department of Earth System Science, University of California, Irvine, California, USA.

<sup>5</sup>Marine Biological Laboratory, Woods Hole, Massachusetts, USA.

**Table 1.** Estimates of DOC Export for the Arctic Basin Used for This Study

Region	Basin	Area ( $10^3 \text{ km}^2$ )	Annual Water Discharge ( $\text{km}^3 \text{ a}^{-1}$ )	DOC Flux ( $\text{Tg C a}^{-1}$ )
1	Arctic Archipelago	1231	204	1.01
2	Barents Sea	1279	446	4.28
3	Beaufort Sea	2090	418	2.54
4	Bering Strait	1218	312	2.30
5	Chukchi Sea	234	121	0.375
6	East Siberian Sea	1345	242	2.40
7	Hudson Bay	3308	635	3.29
8	Hudson Strait	468	237	2.18
9	Kara Sea	6615	1220	11.1
10	Laptev Sea	3632	759	8.26
Total		21,420	4594	37.7

(OGCM) with highly simplified biogeochemical parameterizations, configured in the Arctic Basin. We address the following question: What is the role of the riverine sources and ocean circulation in setting the observed distribution of DOC and DSR in the Arctic Ocean? In addressing this question, we will develop a parameterization of terrigenous DOC which can be applied in global or Arctic Ocean biogeochemistry models. In section 2 we describe the OGCM, the construction of the climatological flux of riverine DOC, the tracer model, and the general experimental design. In section 3, we briefly review the solution of the circulation model and discuss the simulations of, and controls on, the DSR in our numerical experiments. We summarize and examine the broader implications in section 4.

## 2. Methods

### 2.1. Ocean General Circulation Model: Regional Arctic Setup

[4] To drive the tracer and biogeochemical models, we employ simulations of ocean circulation made using the MIT General Circulation Model (MITgcm) [Marshall *et al.*, 1997] with a coupled sea ice model. The model is configured on a “cubed sphere” grid in a limited area Arctic domain with open boundaries at  $\sim 55^\circ\text{N}$  in the Atlantic and Pacific sectors. Prescribed boundary conditions for potential temperature, salinity, flow, and sea surface elevation are provided from previous integrations of a global configuration of the same model [Menemenlis *et al.*, 2005]. The grid is locally orthogonal and has a variable horizontal resolution with an average spacing of  $\sim 18$  km. The mesh resolves major Arctic straits, including many of the channels of the Canadian Archipelago. Since the baroclinic Rossby radius of deformation in the Arctic Ocean is of order 10 km, the 18-km horizontal grid spacing of the model is not eddy resolving. There are many other sub-grid-scale processes, for example, restratification, eddy-bathymetry interactions, and salt plumes, which are not well represented by this model. Nevertheless, the 18-km mesh resolves the major boundary currents, Arctic straits, and channels of the Canadian Archipelago. This model configuration was previously used to study the Arctic freshwater budget [Condrón *et al.*, 2009]. Compared to observations by Serreze *et al.* [2006], modeling studies of Condrón *et al.* [2009] conclude that this

model configuration is able to realistically represent the freshwater budget of the Arctic Ocean, including import and export of fresh water from the Bering and Fram straits and from the Canadian Archipelago. The sea ice and fluid dynamical equations are solved on the same horizontal mesh. The vertical grid is height based, varying from 10 m thick near the surface to  $\sim 450$  m thick at a depth of  $\sim 6$  km in 28 levels. Bathymetry is derived from the U.S. National Geophysical Data Center (NGDC) 2-min global relief data set (ETOPO2), which uses the International Bathymetric Chart of the Arctic Ocean product for Arctic bathymetry. The ETOPO2 data are smoothed to the coupled model horizontal mesh and mapped to the ocean vertical levels using a “lopped cell” strategy [Adcroft *et al.*, 1997], which permits accurate representation of the ocean bottom boundary.

[5] Initial ocean hydrography is taken from the Polar Science Center Hydrographic Climatology (PHC) 3.0 database [Steele *et al.*, 2001]. Initial sea ice distributions are taken from the Pan-Arctic Ice-Ocean Modeling and Assimilation System data sets [Zhang and Rothrock, 2003]. Atmospheric state (10-m surface winds, 2-m air temperatures and humidities, and downward long- and short-wave radiation) is taken from the 6-hourly data sets of the National Centers for Environmental Prediction reanalysis [Kalnay *et al.*, 1996]. Monthly mean estuarine fluxes of fresh water are based on the Arctic runoff database [Lammers *et al.*, 2001; Shiklomanov *et al.*, 2000]. Further details of the circulation model configuration are given in Appendix A.

### 2.2. Parameterization of Riverine DOC Discharge

[6] We estimated the DOC export for 10 domains within the pan-Arctic watershed: (1) Arctic Archipelago, (2) Barents Sea, (3) Beaufort Sea, (4) Bering Strait, (5) Chukchi Sea, (6) East Siberian Sea, (7) Hudson Bay, (8) Hudson Strait, (9) Kara Sea, and (10) Laptev Sea (Table 1 and Figure 1). The domains are defined by Lammers *et al.* [2001] with respect to runoff during December–March, April–July, and August–November. We used empirical relationships quantifying the covariation between discharge and DOC to scale the Lammers *et al.* [2001] discharge estimates into parallel estimates of DOC export. We then divided our December–March, April–July, and August–November estimates of DOC export into monthly bins according to measured distributions of DOC export for those months in Arctic rivers. DOC-discharge relationships were developed for each season, with North American and Eurasian rivers considered separately.

[7] Data from the Yukon, Mackenzie, and Kuparuk rivers were used to develop the North American relationships, whereas data from Yenisey, Ob’, and Lena were used to develop the Eurasian relationships. DOC for the Yenisey, Ob’, Lena, and Mackenzie were collected as part of the Pan-Arctic River Transport of Nutrients, Organic Matter, and Suspended Sediments (PARTNERS) project [McClelland *et al.*, 2008]. DOC for the Kuparuk River were collected as part of the NSF Study of the Northern Alaska Coastal System (SNACS, <http://www.arcus.org/arcss/snacs/index.php>). In all cases, discharge data were acquired from ArcticRIMS (<http://rims.unh.edu/>). The PARTNERS and SNACS efforts both employed sampling programs designed to capture seasonal dynamics in DOC and export. Strong

## Locations of riverine DOC discharge

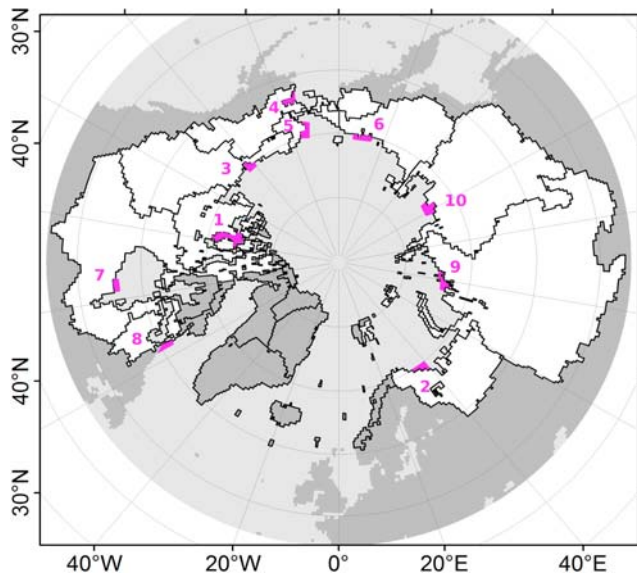


**Figure 1.** Locations of tracer release in the Arctic Ocean according to the distribution of watersheds derived from *Lammers et al.* [2001]. Numbers correspond to the regions listed in Table 1.

positive relationships between DOC and discharge were identified in all of the rivers [*McClelland et al.*, 2007; *Raymond et al.*, 2007; *Holmes et al.*, 2008]. These relationships were then used to estimate daily DOC export from each river. Daily values were then summed over the December–March, April–July, and August–November periods. Finally, all values were normalized by watershed area and incorporated into multiriver ensembles defining general relationships between runoff and DOC export for application in regions without direct DOC measurements. This scaling-up procedure accounts for seasonal and continental scale differences that were not resolved by *Raymond et al.* [2007] when estimating total DOC export from rivers into the Arctic Ocean. For each region that matches the division of the Arctic coastline according to *Lammers et al.* [2001] we calculate the riverine tracer source of DOC ( $RTS_{(DOC)}$ ) as the product between the export of DOC ( $Flux_{(DOC)}$ ) and the discharge area (DA) as follows:

$$RTS_{(DOC)}(t) = Flux_{(DOC)}(t)DA, \quad (1)$$

where the units are  $\text{mol C month}^{-1}$  for  $RTS_{(DOC)}$ ,  $\text{mol C m}^{-2} \text{ month}^{-1}$  for  $Flux_{(DOC)}$ , and  $\text{m}^2$  for DA. For each region of DOC discharge we define a portion of coastal ocean ( $A_T$ ) represented by a contiguous set of grid cells close to or between dominant input locations over which we distribute the source, weighted by grid cell area,  $A_{i,j}$ , relative to the total,  $A_T$ :

$$RTS_{(DOC)}^{A_{i,j}}(t) = RTS_{(DOC)}(t) \frac{A_{i,j}}{A_T}, \quad (2)$$

where  $RTS_{(DOC)}^{A_{i,j}}(t)$  has units  $\text{mol C m}^{-3} \text{ s}^{-1}$ . The monthly values are linearly interpolated to each model time step. For

each selected location mentioned above, we thus apply a discharge of DOC associated with the corresponding fresh water runoff which has an explicit representation of the seasonal cycle, including a marked spring peak (Figure 2). The climatological flux of DOC not only reflects the seasonal asymmetry in the magnitude of the DOC source from the rivers to the ocean but also represents the greater terrestrial input from the Eurasian sector relative to the North American sector. The total imposed riverine flux of DOC to the Arctic Ocean is  $\sim 37 \text{ Tg C a}^{-1}$ , higher than prior estimates because of the inclusion of high spring fluxes and inputs into Hudson Bay.

### 2.3. Idealized Tracer Model

[8] We formulate a suite of idealized tracer experiments to explore the transport and fate of riverine DOC in the model environment. Tracers,  $C$ , are governed by the following prognostic equation:

$$\frac{\partial C}{\partial t} = -u \cdot \nabla C + \nabla \cdot K \nabla C + RTS(x,y,t) - \lambda C, \quad (3)$$

where the first term on the right-hand side is advection by the modeled ocean currents, the second term is sub-grid-scale mixing parameterized as a diffusion tensor, the third term is the riverine source of tracer (described above for DOC), and the last term a simple linear decay, with e-folding lifetime  $\tau = 1/\lambda$ , where  $\lambda$  ( $\text{s}^{-1}$ ) is the DOC decay rate. This is a highly idealized parameterization of the microbial respiration of DOC. Tracers are transported using a third-order upwind advection scheme and may be advected out of the domain at the open boundaries. The tracer concentration is set to zero in waters coming into the domain across the open boundaries. In this idealized study, it is important to note that we do not explicitly take into account the in situ marine production of DOC or the release/sequestration of DOC associated with seasonal melting/formation of sea ice, or DOC contributed by meteoric precipitation falling directly on the ocean surface (see the discussion in section 3.2). We integrate the model for 3 decades after which time tracer distributions are relatively steady; the flushing time for tracers through the surface waters of the basin is on the order of a decade. The physical model is forced with observed meteorological products for the period from 1992 to 2001, and we repeatedly cycle through that period while the tracer fields continue to develop. We illustrate integrations with three tracers, each with DOC-like riverine sources, including a passive tracer ( $\tau$  is infinite) and two DOC-like tracers with  $\tau$  equal to 7 and 10 years.

## 3. Results and Discussion

### 3.1. Modeled Surface Circulation

[9] The ocean model plausibly captures the main features of the large-scale circulation of the Arctic Ocean including the four major components of the basin-scale surface flow: (1) the inflow of North Atlantic Waters into the Arctic Ocean, following the Eurasian side of the basin and continuing along the North American side; (2) the inflow of surface Pacific waters through the Bering Strait, contributing to the Transpolar Drift that flows across the basin and

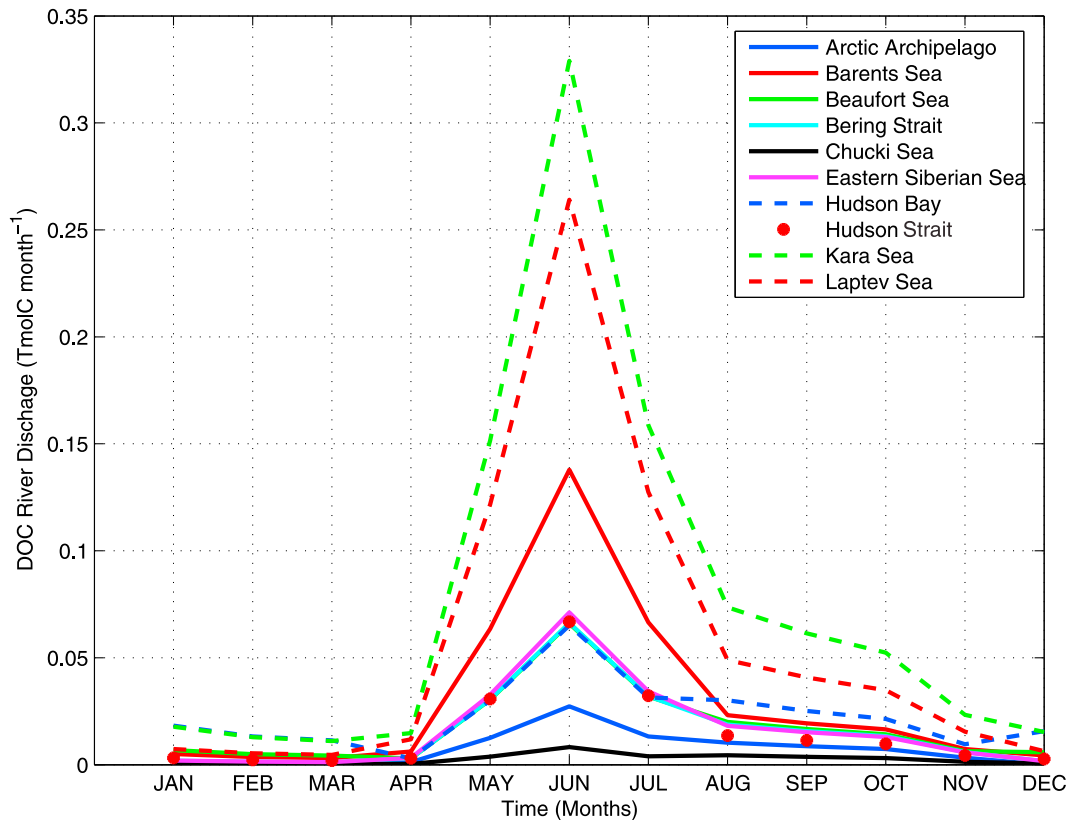


**Figure 2.** Seasonal cycle of riverine DOC discharge for the main rivers implemented in the regional Arctic setup of MITgcm used for this study. Discharge locations correspond to those listed in Table 1, and their positions are shown in Figure 1.

around the North American coast (the Transpolar Drift also has a contribution from the recirculation of waters of Atlantic origin); (3) the outflow through the Denmark and Fram straits and along the Canadian coast and Hudson Strait; and (4) inside the Arctic Basin, closer to the North American side, the recirculating Beaufort Gyre. The modeled distribution of sea surface salinity (SSS) (Figure 3) reveals key water masses and pathways of the Arctic Basin. The North Atlantic waters enter the basin with high salinity ( $SSS \approx 34.8$  psu) and are progressively diluted by interior surface ( $SSS \approx 32$  psu) and coastal waters ( $SSS < 24$  psu) as they penetrate into the Arctic Basin. Surface Pacific waters are characterized by typical SSS values of 32 psu, considerably fresher than the those entering from the Atlantic side (Figure 3). The passive tracer of riverine origin clearly tracks the interaction of water masses with the surface waters of Atlantic origin flowing along the Eurasian coast then becoming entrained in the Transpolar Drift (TPD) (Figure 4). The transit of the surface Pacific waters is revealed by their association with low tracer concentrations (Figure 4) due to the relatively small source outside the Bering Strait (note that we do not explicitly represent the open ocean “background” or in situ production of DOC in these idealized experiments). On the North American side of the basin, the Mackenzie River enriches the surface Pacific waters with tracers of riverine source.

[10] The tracer distribution (Figure 4) indicates that the tracer of riverine origin is transported toward the North

Atlantic when incorporated in the flow of the Eastern Greenland Current, consistent with the interpretation of *Benner et al.* [2005], who reported that the Eastern Greenland Current alone exports 4.6–6.6 Tg C of terrigenous origin from the Arctic Ocean to the North Atlantic. Similar results have also been found in a modeling study by *Newton et al.* [2008].

### 3.2. DOC-Salinity Relationship in the Arctic Ocean

[11] Since the circulation model captures the essence of the large-scale patterns of surface circulation (at least in this period of predominantly high North Atlantic Oscillation (NAO) index [*Hurrell, 1995; Condron et al., 2009*]), we will use this framework to simulate regional DSRs and ask if the model can reproduce the observed relationships with terrigenous sources of DOC. If so, what is the value for the lifetime with respect to microbial degradation,  $\tau$ , which best captures the observed relationships?

[12] *Hansell et al.* [2004], combining their observations with those of *Amon and Benner* [2003], showed that the eastern and western sectors of the Arctic Ocean are characterized by two different linear DSRs, as follows:

$$DOC_{(EA)} = (-14.82)\text{salinity} + (596), \quad (4)$$

$$DOC_{(WA)} = (-2.6)\text{salinity} + (154), \quad (5)$$



# Sea Surface Salinity

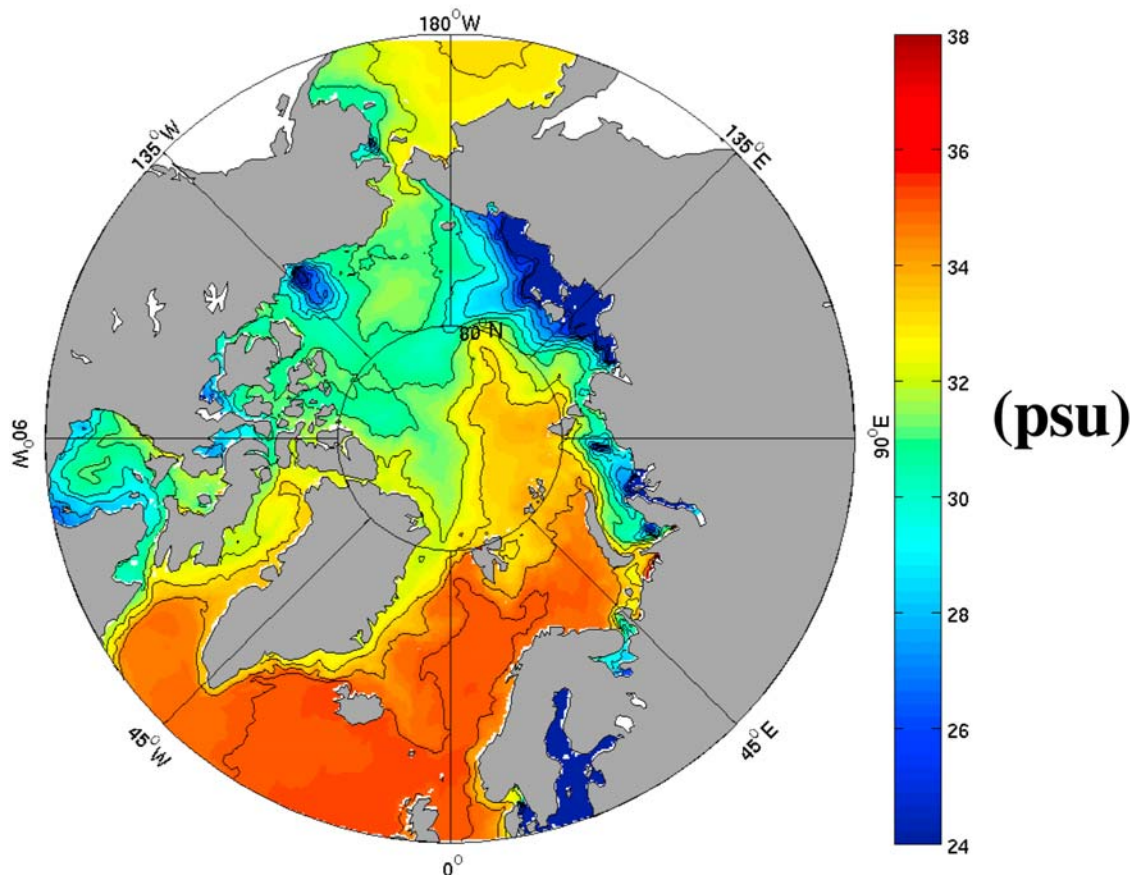


**Figure 3.** Annual average of sea surface salinity. Values refer to the 30th simulated year. Units are psu.

where EA and WA stand for eastern Arctic and western Arctic, respectively. Here we examine the DSR for each of the three modeled tracers ( $\tau = \text{infinity}$ , 10, and 7 years) in surface waters of the eastern and western Arctic of the model. We sample both the simulated tracer concentration and salinity in two regions of the modeled Arctic domain reflecting those where the observations presented by *Hansell et al.* [2004] were made (Figure 4, white boxes).

[13] We consider two aspects of the modeled DSRs in relation to the observations: the absolute abundance of [DOC] and the slope of the linear relationship between [DOC] and salinity. The observed [DOC] distributions reveal no surface waters in either western or eastern Arctic with concentrations less than  $50 \mu\text{M}$ , yet all of the modeled DOC-like tracers have minimum values close to zero. This is because we have not explicitly modeled the in situ production of DOC in the ocean, nor its transport into the Arctic Basin from the Atlantic and Pacific basins. In situ measurements in the global oceans (including the Arctic) [*Anderson, 2002; Benner et al., 2005; Mathis et al., 2005*] suggest a relatively uniform background concentration of refractory DOC between  $40$  and  $50 \mu\text{M}$  throughout, with regional and seasonal variations, particularly in the surface

waters. In order to discuss the Arctic gradients, and whether riverine sources can account for them, for further comparison we simply add a nominal  $50 \mu\text{M}$  “refractory DOC” component to the modeled tracer values.

[14] Figure 5 illustrates the DSR for each of the three modeled tracers (with refractory DOC offset added to modeled tracer results) in the surface waters of the model in eastern and western Arctic subdomains. There is a notable difference in the modeled passive tracer (Figure 5, top left), where  $\tau = \text{infinity}$ , and the observed relationship, particularly in the eastern Arctic region where the tracer values are much higher than the observed DOC. Without a sink, the riverine DOC sources overpredict the measured Arctic DOC. Mixing and dilution alone are insufficient to account for the observed DSR.

[15] The tracers with noninfinite  $\tau$  exhibit more realistic DOC-tracer concentrations and DSRs; of those, the tracer with  $\tau = 10$  years shows the closest correspondence to the observed slopes (Figure 5, bottom right). This is in accord with the inferences of *Hansell et al.* [2004]. The model results are generally consistent with the observed DSR relationships even though we have not represented sea ice freezing/melting or meteoric sources explicitly in the

## Surface Passive [Tracer]

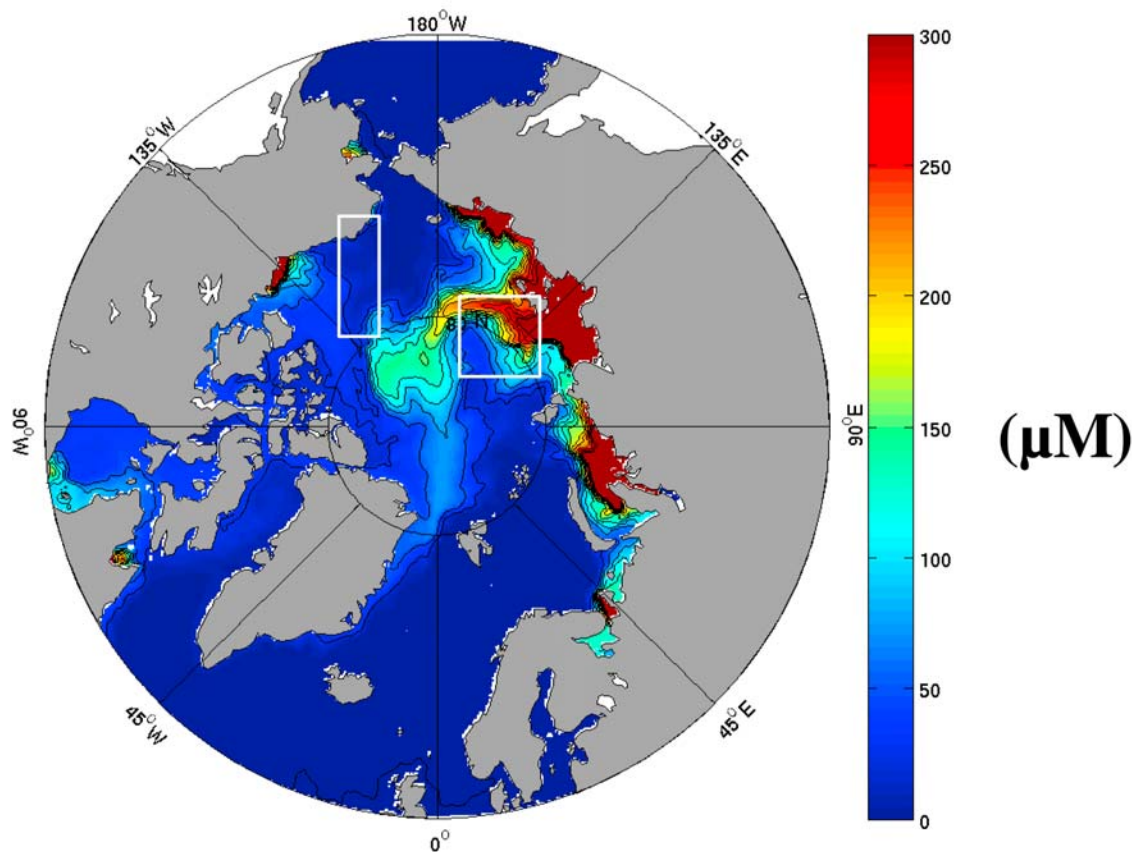


**Figure 4.** Annual average of surface concentration of passive tracer in the 30th simulated year. Units are  $\mu\text{M}$ . Boxes indicate the sampling areas (for salinity and tracer concentration) in the eastern and western sectors of the Arctic Ocean.

parameterization of DOC dynamics. This is consistent with scaling arguments which suggest that these influences are overpowered by the riverine sources, transport, and remineralization. On the basis of data collected in the Arctic Ocean, *Anderson* [2002] suggested that the process of sea ice melting would change the DOC not more than  $6 \mu\text{M kg}^{-1}$ . *Willey et al.* [2000] reported that the amount of DOC associated to the precipitation over the ocean has been estimated between 7 and  $24 \mu\text{M}$  in the Northern Hemisphere. This contrasts, for example, with changes in the modeled DOC of up to  $200 \mu\text{M}$  in the eastern sector of the Arctic Ocean in response to changes in the remineralization rate. Note that we have plotted values corresponding to all the months while the relationship used by *Hansell et al.* [2004] has been calculated only using summer values.

[16] The model results show an essentially linear relationship between salinity and riverine DOC, as shown by observations (fresh, DOC-rich coastal waters versus saline, DOC-poor, open ocean waters), suggesting that the mixing of the two end-members may be an approximate interpretation. We could also consider a multiple end-member scenario with, for example, an additional DOC-poor, fresh, ice melt end-member. However, such a situation is not

clearly identified in the data shown by *Hansell et al.* [2004]. Additionally, using  $\delta^{18}\text{O}$  data, *Cooper et al.* [2005] demonstrated that the spring samples from the western Arctic contained negligible freshwater from sea ice suggesting that the river runoff was the dominant factor.

[17] As is observed, there are distinct and different DSRs in the eastern and western Arctic. Why are there different mean concentrations of terrigenous DOC and different DSRs in the eastern and western basins? Three factors potentially contribute: mixing and circulation, regional differences in riverine sources, and regional difference in quality of the organic material and its remineralization rate. Circulation is certainly important. The TPD cuts through the basin, effectively separating the eastern and western water masses. Tracers of riverine origin are stirred within the eastern and western basins but are advected out of the domain relatively quickly with respect to exchange between the water masses (under positive NAO conditions). This is consistent with the surface salinity distribution and the distinct DOC properties. In a preliminary configuration of the circulation model, which had simpler freshwater boundary conditions, the TPD was much weaker, and mixing between the eastern and western Arctic surface water

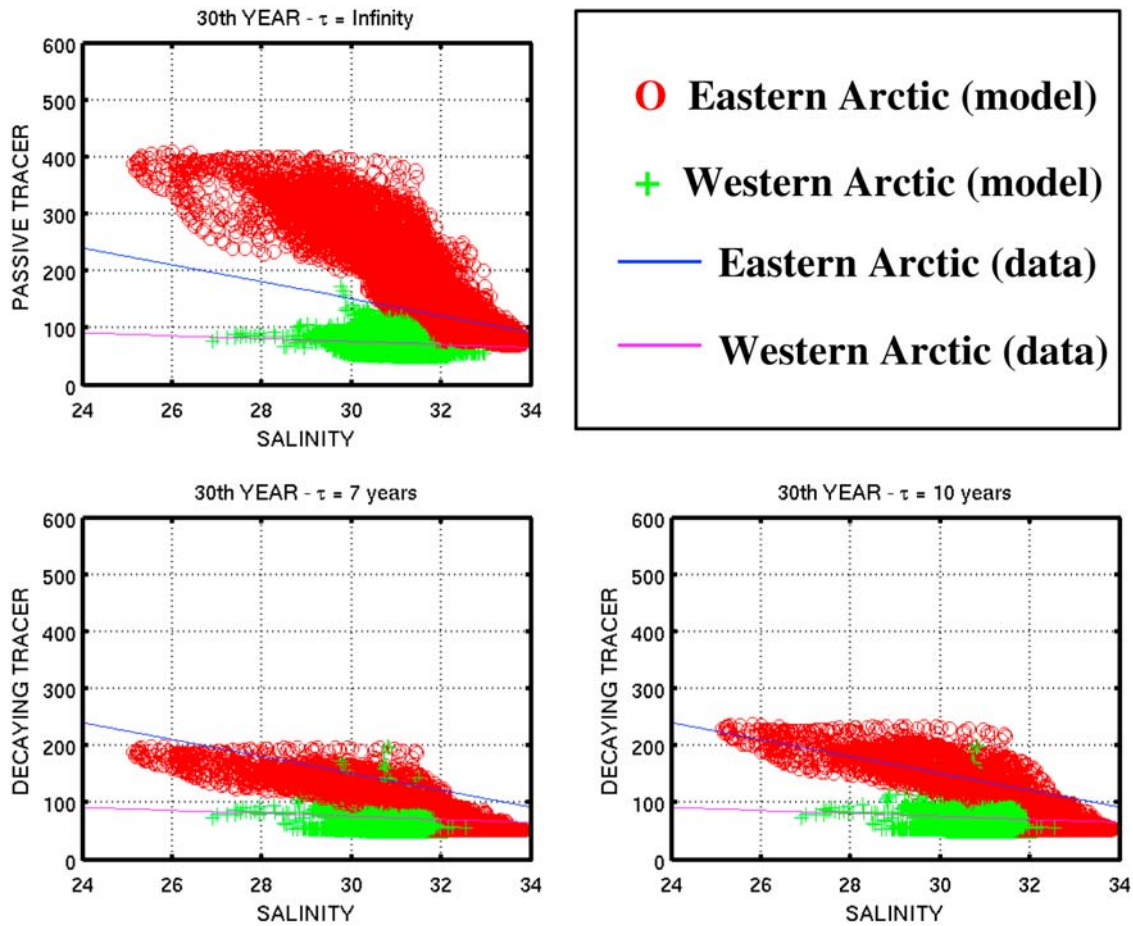


**Figure 5.** Scatterplot of DOC-salinity relationship from model output corrected with addition of the missing refractory contribution ( $50 \mu\text{M}$ ). Parts refer to numerical experiments with values of  $\tau$  of (top left) infinity, (bottom left) 7 years, and (bottom right) 10 years. Straight lines represent the DSR for the (blue) eastern and (magenta) western sectors of the Arctic Ocean obtained by *Hansell et al.* [2004] using field data. Red open circles correspond to modeled values sampled in the eastern Arctic sector, whereas green crosses correspond to modeled values sampled in the western Arctic sector. Plotted values correspond to the white boxes inside the Arctic domain illustrated in Figure 4. Cumulative plots refer to monthly model output from the last simulated year in the first level of our OGCM. Units are  $\mu\text{M}$  for tracer and psu for salinity.

masses of the model was enhanced (not illustrated). In that case, the distinct regional DSRs seen in both the observations and the illustrated models were unrealistically blurred by mixing between eastern and western basins. The data used for evaluating our model results were collected in the 1997/1998 period for the eastern Arctic and in 2002 for the western Arctic. Our numerical simulations cover the period 1992–2001. Over most of this period encompassing both model simulations and observations the system was in a high-NAO state. Why is the mean concentration higher in the eastern basin? We formulate a simple model describing the time evolution of DOC in either the eastern or western basin to address this question:

$$\frac{d\text{DOC}}{dt} = -\lambda\text{DOC} - \Psi(\text{DOC} - \text{DOC}^*) + \text{RS}_{\text{DOC}}. \quad (6)$$

The rate of change of DOC in the subbasin is a balance between its consumption (governed by  $\lambda$ ), exchange of

waters between the local subbasin and surrounding waters with concentration of terrigenous DOC,  $\text{DOC}^*$  ( $\Psi$  being the mixing rate between water masses), and the strength of the local riverine source,  $\text{RS}_{\text{DOC}}$ . Considering the large gradient of DOC between open ocean and the coastal zone, we assume that

$$\text{DOC} \gg \text{DOC}^*, \quad (7)$$

and steady state solution ( $d\text{DOC}/dt = 0$ ) is

$$\text{DOC} = \frac{\text{RS}_{\text{DOC}}}{\lambda + \Psi}. \quad (8)$$

This simple equation qualitatively suggests that in the subbasins, surface DOC is proportional to the strength of the local riverine source and inversely proportional to the rate of remineralization,  $\lambda$ , and the rate of physical mixing

( $\Psi$ ). The contrast in the modeled DOC of the eastern and western basins seems realistic and, since a uniform  $\lambda$  is imposed, does not depend on variations in the remineralization rate. Tracer observations suggest that the residence time of waters is greater in the western basin (i.e.,  $\Psi$  is lower) than in the eastern. This simple model (equation (8)) would then suggest that [DOC] should be larger in the western basin, but our results indicate that the significantly greater riverine source into the eastern subbasin dominates.

[18] The success of the model in capturing the separate eastern and western DSRs suggests that the physical model faithfully captures key features of the Arctic circulation and that provided the uniform remineralization rate is appropriate, the model of riverine sources is appropriate. Our study suggests that it is the role of the Transpolar Drift as a barrier to mixing and the stronger riverine sources on the eastern shore that drive the cross-basin differences in mean DOC and DSR.

#### 4. Summary

[19] We have developed a parameterization of the riverine fluxes of terrigenous DOC into the Arctic Basin and implemented it in a regional model of ocean circulation, tracer transport, and simplified biogeochemistry. When the global background of refractory DOC is accounted for, and assuming a simple  $e$ -folding lifetime of 10 years for terrigenous DOC in the ocean, we are able to simulate the large-scale distribution and relationship to salinity of [DOC] in the Arctic without considering in situ local production. This is consistent with previous interpretations of observations [Hansell *et al.*, 2004] and provides the basis for a parameterization of terrigenous DOC for regional or global carbon cycle models.

[20] The model captures the observed, distinct DSRs and contrast in mean DOC in the eastern and western Arctic. Sensitivity studies and the analytical construct equation (8) suggest that this contrast is maintained by the Transpolar Drift, acting as a barrier to mixing (at least in the positive phase of the North Atlantic Oscillation), and the difference in the strength of riverine sources across the basin.

[21] In fact, we have simulated the period 1992–2001, corresponding to a positive phase of the NAO. Modeling studies [Proshutinsky and Johnson, 1997; Condrón *et al.*, 2009] suggest that the phase of the NAO (either positive or negative) can substantially influence the surface circulation of the Arctic Ocean, which could also impact the transport and fate of riverine DOC or any other tracer in the top layers of the ocean influenced by the wind direction and strength [Condrón *et al.*, 2009]. One of the main differences between the positive and negative NAO phases in the Arctic Ocean circulation is the strength of the Beaufort Gyre. The strength of this specific circulation feature could impact the residence time of DOC in the Arctic Basin and the mixing of end-member water masses from the two sides of the Arctic Basin.

[22] It is natural to ask next, what is the impact of the terrigenous sources on the regional air-sea flux of CO<sub>2</sub> and export of carbon to the Atlantic basin [Anderson *et al.*, 1998]? The data presented by Benner *et al.* [2005] suggest

that the Eastern Greenland Current could impact the air-sea fluxes of CO<sub>2</sub> in the subpolar North Atlantic because of the supply of riverine carbon coming from the Arctic Ocean. Here we have developed a parameterization of riverine DOC sources and sinks which can be used to address this question in the context of a regional ocean carbon cycle model.

#### Appendix A: Circulation Model Parameters

[23] The ocean component is configured to use an equation of state formulated according to Jackett and McDougall [1995]. Ocean surface fluxes (in the absence of sea ice) are calculated using bulk formula according to Large and Pond [1981]. Boundary layer and convective mixing in the ocean is parameterized according to Large *et al.* [1994]. Background vertical diffusivity of temperature and salinity is set to  $3.6 \times 10^{-6} \text{ m}^2 \text{ s}^{-1}$ . An enhanced vertical diffusivity of  $1.1 \times 10^{-4} \text{ m}^2 \text{ s}^{-1}$  is active at depth motivated by Bryan and Lewis [1979]. Tracer transport equations are solved using a high-order monotonicity-preserving scheme [Daru and Tenaud, 2004]. Nonlinear momentum terms are solved using a vector invariant formulation according to Adcroft *et al.* [2004] with viscous dissipation following Leith [1968] but modified to dissipate divergence as well as vorticity [Fox-Kemper and Menemenlis, 2008].

[24] The sea ice component of the coupled system follows the viscous plastic rheology formulation of Hibler [1979] with momentum equations solved implicitly on a C grid [Arakawa and Lamb, 1977] using a procedure based on the work of Zhang and Hibler [1997]. Fluxes of momentum into ice due to the overlying atmospheric winds and momentum fluxes between sea ice and the ocean are calculated by solving for the momentum balance at each surface grid column [Hibler and Bryan, 1987]. The freezing and melting of sea ice and associated fluxes of heat and fresh water between the ocean, sea ice, and atmosphere are calculated by solving a heat balance equation for each surface grid column at each time step [Zhang *et al.*, 1998; Hibler, 1980; Parkinson and Washington, 1979; Semtner, 1976]. The ocean sea ice coupled system is stepped forward synchronously with a time step of 1800 s.

[25] **Acknowledgments.** This study has been carried out in the framework of the ECCO2 Project (<http://ecco2.org>), and it is also part of the project Synthesis of Arctic System Science I.M.M. and M.J.F. are grateful to National Science Foundation for financial support. M.M. thanks Jean-Michel Campin and Baylor Fox-Kemper for their valuable help with MITgcm, Alan Condrón for useful discussions on Arctic circulation, and NASA for providing excellent support for scientific computation. We also thank Dennis Hansell and Nicholas Bates for constructive comments and guidance during the development of this study. Comments from two anonymous reviewers helped us to improve the weak parts of the initial version of our manuscript.

#### References

- Adcroft, A., C. Hill, and J. Marshall (1997), Representation of topography by shaved cells in a height coordinate ocean model, *Mon. Weather Rev.*, *125*, 2293–2315, doi:10.1175/1520-0493(1997)125<2293:ROTBS>2.0.CO;2.
- Adcroft, A., J.-M. Campin, C. Hill, and J. Marshall (2004), Implementation of an atmosphere-ocean general circulation model on the expanded spherical cube, *Mon. Weather Rev.*, *132*, 2845–2863, doi:10.1175/MWR2823.1.



- Amon, R. M. W., and R. Benner (1996), Bacterial utilization of different size classes of dissolved organic matter, *Limnol. Oceanogr.*, *41*, 41–51.
- Amon, R. M. W., and R. Benner (2003), Combined neutral sugars as indicators of the diagenetic state of dissolved organic matter in the Arctic Ocean, *Deep Sea Res., Part I*, *50*, 151–169, doi:10.1016/S0967-0637(02)00130-9.
- Anderson, L. G. (2002), DOC in the Arctic Ocean, in *Biogeochemistry of Marine Dissolved Organic Matter*, edited by D. A. Hansell and C. A. Carlson, pp. 665–683, Elsevier Sci., Boston, Mass.
- Anderson, L. G., K. Olson, and M. Chierici (1998), A carbon budget for the Arctic Ocean, *Global Biogeochem. Cycles*, *12*(3), 455–465, doi:10.1029/98GB01372.
- Arakawa, A., and V. Lamb (1977), Computational design of the basic dynamical processes of the UCLA general circulation model, *Methods Comput. Phys.*, *17*, 174–267.
- Azam, F., and R. E. Hodson (1977), Size distribution and activity of marine microheterotrophs, *Limnol. Oceanogr.*, *22*, 492–501.
- Benner, R., P. Louchouart, and R. M. W. Amon (2005), Terrigenous dissolved organic matter in the Arctic Ocean and its transport to surface and deep waters of the North Atlantic, *Global Biogeochem. Cycles*, *19*, GB2025, doi:10.1029/2004GB002398.
- Bryan, K., and L. J. Lewis (1979), A water mass model of the world ocean, *J. Geophys. Res.*, *84*(C5), 2503–2517, doi:10.1029/JC084iC05p02503.
- Condon, A., P. Winsor, C. N. Hill, and D. Menemenlis (2009), Response of Arctic freshwater budget to extreme NAO forcing, *J. Clim.*, *22*, 2422–2437, doi:10.1175/2008JCLI2626.1.
- Cooper, L. W., R. Benner, J. W. McClelland, B. J. Peterson, R. M. Holmes, P. A. Raymond, D. A. Hansell, J. M. Grebmeier, and L. Codispoti (2005), Linkages among runoff, dissolved organic carbon, and the stable oxygen isotope composition of seawater mass indicators in the arctic ocean, *J. Geophys. Res.*, *110*, G02014, doi:10.1029/2005JG000031.
- Daru, V., and C. Tenaud (2004), High order one-step monotonicity-preserving schemes for unsteady compressible flow calculations, *J. Comput. Phys.*, *193*(2), 563–594, doi:10.1016/j.jcp.2003.08.023.
- Dittmar, T., and G. Kattner (2003), The biogeochemistry of the river and shelf ecosystem of the Arctic Ocean: A review, *Mar. Chem.*, *83*, 103–120, doi:10.1016/S0304-4203(03)00105-1.
- Dixon, R. K., A. M. Solomon, S. Brown, R. A. Houghton, M. C. Trexler, and J. Wisniewski (1994), Carbon pools and flux of the global forest ecosystem, *Science*, *263*, 185–190, doi:10.1126/science.263.5144.185.
- Fox-Kemper, B., and D. Menemenlis (2008), Can large eddy simulation techniques improve mesoscale rich ocean models?, in *Ocean Modeling in an Eddy Regime*, *Geophys. Monogr. Ser.*, vol. 177, edited by M. W. Hecht and H. Hasumi, pp. 319–338, AGU, Washington, D. C.
- Gordeev, V. V., J. M. Martin, I. S. Sidorov, and M. V. Sidorova (1996), A reassessment of the Eurasian river input of water, sediment, major elements, and nutrient in the Arctic Ocean, *Am. J. Sci.*, *296*, 664–691.
- Hansell, D. A., D. Kadko, and N. R. Bates (2004), Degradation of terrigenous dissolved organic carbon in the western Arctic Ocean, *Science*, *304*, 858–861, doi:10.1126/science.1096175.
- Hibler, W. D., III (1979), A dynamic thermodynamic sea ice model, *J. Phys. Oceanogr.*, *9*, 815–846, doi:10.1175/1520-0485(1979)009<0815:ADTSIM>2.0.CO;2.
- Hibler, W. D., III (1980), Modeling a variable thickness sea ice cover, *Mon. Weather Rev.*, *1*, 1943–1973, doi:10.1175/1520-0493(1980)108<1943:MAVTSI>2.0.CO;2.
- Hibler, W. D., III, and K. Bryan (1987), A diagnostic ice-ocean model, *J. Phys. Oceanogr.*, *17*, 987–1015, doi:10.1175/1520-0485(1987)017<0987:ADIM>2.0.CO;2.
- Holmes, R. M., J. W. McClelland, P. A. Raymond, B. B. Frazer, B. J. Peterson, and M. Stieglitz (2008), Liability of DOC transported by Alaskan rivers to the Arctic Ocean, *Geophys. Res. Lett.*, *35*, L03402, doi:10.1029/2007GL032837.
- Hurrell, J. W. (1995), Decadal trends in the North-Atlantic oscillation: Regional temperatures and precipitations, *Science*, *269*, 676–679, doi:10.1126/science.269.5224.676.
- Jackett, D. R., and T. J. McDougall (1995), Minimal adjustment of hydrographic profiles to achieve static stability, *J. Atmos. Oceanic Technol.*, *12*(4), 381–389, doi:10.1175/1520-0426(1995)012<0381:MAOHT>2.0.CO;2.
- Kalnay, E., et al. (1996), The NCEP/NCAR 40-year reanalysis project, *Bull. Am. Meteorol. Soc.*, *77*, 437–471, doi:10.1175/1520-0477(1996)077<0437:TNYRP>2.0.CO;2.
- Kieber, R. J., X. Zhou, and K. Mopper (1990), Formation of carbonyl compounds from UV-induced photodegradation in marine waters: Fate of riverine carbon in the sea, *Limnol. Oceanogr.*, *35*, 1503–1515.
- Lammers, R. B., A. I. Shiklomanov, C. J. Vorösmarty, B. M. Fekete, and B. J. Peterson (2001), Assessment of contemporary Arctic river runoff based on observational discharge records, *J. Geophys. Res.*, *106*(D4), 3321–3334, doi:10.1029/2000JD900444.
- Large, W. G., and S. Pond (1981), Open ocean momentum flux measurements in moderate to strong winds, *J. Phys. Oceanogr.*, *11*, 324–336, doi:10.1175/1520-0485(1981)011<0324:OOMFMI>2.0.CO;2.
- Large, W. G., J. McWilliams, and S. Doney (1994), Oceanic vertical mixing: A review and a model with nonlocal boundary layer parameterization, *Rev. Geophys.*, *32*, 363–403, doi:10.1029/94RG01872.
- Leith, C. E. (1968), Diffusion approximation for two-dimensional turbulence, *Phys. Fluids*, *11*, 671, doi:10.1063/1.1691968.
- Lobbes, J., H. P. Fitznar, and G. Kattner (2000), Biogeochemical characteristics of dissolved and particulate organic matter in Russian rivers entering the Arctic Ocean, *Geochim. Cosmochim. Acta*, *64*, 2973–2983, doi:10.1016/S0016-7037(00)00409-9.
- Marshall, J., C. Hill, L. Perelman, and A. Adcroft (1997), Hydrostatic, quasi-hydrostatic, and nonhydrostatic ocean modeling, *J. Geophys. Res.*, *102*(C3), 5733–5752, doi:10.1029/96JC02776.
- Mathis, J. T., D. A. Hansell, and N. R. Bates (2005), Strong hydrographic controls on spatial and seasonal variability of dissolved organic carbon in Chukchi Sea, *Deep Sea Res., Part II*, *52*, 3245–3258, doi:10.1016/j.dsr2.2005.10.002.
- McClelland, J. W., M. Stieglitz, F. Pan, R. M. Holmes, and B. J. Peterson (2007), Recent changes in nitrate and dissolved organic carbon export from the upper Kuparuk River, North Slope, Alaska, *J. Geophys. Res.*, *112*, G04S60, doi:10.1029/2006JG000371.
- McClelland, J. W., et al. (2008), Development of a pan-Arctic database for river chemistry, *Eos Trans. AGU*, *89*(24), 217, doi:10.1029/2008EO240001.
- Menemenlis, D., et al. (2005), NASA supercomputer improves prospects for ocean climate research, *Eos Trans. AGU*, *86*(9), 89, doi:10.1029/2005EO090002.
- Newton, R., P. Schlosser, D. G. Martinson, and W. Maslowski (2008), Freshwater distribution in the arctic ocean: Simulation with high-resolution model and model-data comparison, *J. Geophys. Res.*, *113*, C05024, doi:10.1029/2007JC004111.
- Opsahl, S., R. Benner, and R. Amon (1999), Major flux of terrigenous organic matter through the Arctic Ocean, *Limnol. Oceanogr.*, *44*, 2017–2023.
- Parkinson, C. L., and W. M. Washington (1979), A large-scale numerical of sea ice, *J. Geophys. Res.*, *84*(C1), 311–337, doi:10.1029/JC084iC01p00311.
- Proshutinsky, A. Y., and M. A. Johnson (1997), Two circulation regimes of the wind-driven Arctic Ocean, *J. Geophys. Res.*, *102*(C6), 12,493–12,514, doi:10.1029/97JC00738.
- Raymond, P. A., J. McClelland, R. Holmes, A. Zhulidov, K. Mull, B. Peterson, R. Striegl, G. Aiken, and T. Gurtovaya (2007), Flux and age of dissolved organic carbon exported to the arctic ocean: A carbon isotopic study of the five largest arctic rivers, *Global Biogeochem. Cycles*, *21*, GB4011, doi:10.1029/2007GB002934.
- Semtner, A. J., Jr. (1976), A model for the thermodynamic growth of sea ice in numerical investigations of climate, *J. Phys. Oceanogr.*, *6*, 379–389, doi:10.1175/1520-0485(1976)006<0379:AMFTTG>2.0.CO;2.
- Serreze, M., A. P. Barret, A. G. Slater, R. A. Woodgate, K. Aagard, R. B. Lammers, M. Steele, R. Mortiz, M. Meredith, and C. M. Lee (2006), The large-scale fresh water cycle of the Arctic, *J. Geophys. Res.*, *111*, C11010, doi:10.1029/2005JC003424.
- Shiklomanov, I., A. Shiklomanov, R. Lammers, B. Peterson, and C. Vorösmarty (2000), The dynamics of river water inflow to the Arctic Ocean, in *The Freshwater Budget of the Arctic Ocean*, edited by E. Lewis, pp. 281–296, Kluwer Acad., Boston, Mass.
- Steele, M., R. Morley, and W. Ermold (2001), PHC: A global ocean hydrography with a high quality Arctic Ocean, *J. Clim.*, *14*, 2079–2087, doi:10.1175/1520-0442(2001)014<2079:PAGOHV>2.0.CO;2.
- Stein, R., and R. W. MacDonald (Eds.) (2003), *The Organic Carbon Cycle in the Arctic Ocean*, 363 pp., Springer, New York.
- Willey, J. D., R. J. Kieber, M. S. Eymann, and G. B. Avery Jr. (2000), Rainwater dissolved organic carbon: Concentrations and global flux, *Global Biogeochem. Cycles*, *14*(1), 139–148, doi:10.1029/1999GB900036.
- Zhang, J., and W. D. Hibler III (1997), On an efficient numerical method for modeling sea ice dynamics, *J. Geophys. Res.*, *102*(C4), 8691–8702, doi:10.1029/96JC03744.
- Zhang, J., and D. Rothrock (2003), Modeling global sea ice with a thickness and enthalpy distribution model in generalized curvilinear coordinates, *Mon. Weather Rev.*, *131*, 845–861, doi:10.1175/1520-0493(2003)131<0845:MGSIIWA>2.0.CO;2.
- Zhang, J., W. D. Hibler III, M. Steele, and D. A. Rothrock (1998), Arctic ice-ocean modeling with and without climate restoring, *J. Phys. Oceanogr.*

28, 191–217, doi:10.1175/1520-0485(1998)028<0191:AIOMWA>2.0.CO;2.

---

S. Dutkiewicz, M. J. Follows, C. N. Hill, and M. Manizza, Department of Earth, Atmospheric, and Planetary Sciences, Massachusetts Institute of Technology, 77 Massachusetts Avenue, Cambridge, MA 01239, USA. (mmanizza@ocean.mit.edu)

J. W. McClelland, Marine Science Institute, University of Texas at Austin, 750 Channel View Drive, Port Aransas, TX 78373, USA.

D. Menemenlis, Jet Propulsion Laboratory, California Institute of Technology, 4800 Oak Grove Drive, Pasadena, CA 91109-8099, USA.

B. J. Peterson, Marine Biological Laboratory, 7 MBL Street, Woods Hole, MA 02543, USA.

A. Townsend-Small, Department of Earth System Science, University of California, Irvine, 2313 Croul Hall, Irvine, CA 92697-3100, USA.